*Progress In Electromagnetics Research, PIER 69, 201–217, 2007*

# AN UNCONDITIONALLY STABLE PRECISE INTEGRATION TIME DOMAIN METHOD FOR THE NUMERICAL SOLUTION OF MAXWELL'S EQUATIONS IN CIRCULAR CYLINDRICAL COORDINATES

**X.-T. Zhao, X.-K. Ma, and Y.-Z. Zhao**

Department of Electrical Engineering
Xi'an Jiaotong University
Xi'an, 710049, P. R. China

**Abstract**—The extension of an unconditionally stable precise integration time domain method for the numerical solutions of Maxwell's equations to circular cylindrical coordinate system is presented in this paper. In contrast with the conventional cylindrical finite-difference time-domain method, not only can it remove the Courant stability condition constraint, but also make the numerical dispersion independent of the time-step size. Moreover, the first-order absorbing boundary condition can be introduced into the proposed method successfully, whereas the alternating-direction-implicit finite-difference time-domain method may become instable for open region radiation problems terminated with absorbing boundary conditions. Theoretical proof of the unconditional stability is mentioned and the numerical results are presented to demonstrate the effectiveness of the proposed method in solving electromagnetic-field problem.

## 1. INTRODUCTION

The finite-difference time-domain (FDTD) method [1] has been widely used in solving electromagnetic problems due to its capability of precise predictions of field behaviors [2–5]. By finite-differencing Maxwell's equations, the field solutions at a current time step are deduced from the field values at the previous time steps in a recursive fashion. This recursive scheme can provide field information in both time and frequency domains over a large bandwidth if the excitation is of large bandwidth. The detailed theory and extensive applications are described in [6].

Although the FDTD is an effective method in solving electromagnetic problems, there are inherent modeling constraints that limit its applications to electrically small structures. One of them is the Courant stability condition. It requires that a time step must be smaller than a certain limit to ensure numerical stability. For a conventional cylindrical FDTD method [7, 8], the time step $\tau$ has to satisfy the following stability condition

$$\tau \leq \tau_c = \left\{ v_{\max} \sqrt{(1/\Delta r)^2 + [2/(\Delta r \Delta \varphi)]^2 + (1/\Delta z)^2} \right\}^{-1} \tag{1}$$

where $v_{\max}$ is the maximum phase velocity in the media being modeled, $\Delta r, \Delta\varphi$, and $\Delta z$ are the smallest spatial discretization steps in the radial, angular, and vertical directions, respectively. Equation (1) indicates that the time-step limit is related to the spatial steps, as well as medium constitutive parameters.

Various time-domain techniques have been developed to improve the FDTD computation efficiency. One of them is the very recently developed alternating-direction-implicit FDTD [9, 10]. It removes the stability constraint successfully. But larger time steps will affect the numerical phase velocity, and the dispersion errors increase when the time steps increase [11]. Moreover, some research works show that in open region radiation problems, in which a mesh-truncation technique or absorbing boundary condition is applied, the method can become instable [12, 13].

The precise integration technique was first used in calculating the transient responses of transmission lines, and in modeling the effects of interconnects in high-speed VLSI [14, 15]. Then, this method is used to analyze the electromagnetic pulse propagation in conductive nonlinear magnetic materials [16]. However, these works are focused on the 1-D problems. Recently, such principle as applied in [14–16] is extended to three dimensions, and a 3-D precise integration time domain method that is free of the Courant stability condition is consequently developed in Cartesian coordinates [17, 18]. In it, the precise integration technique is applied to the Yee's staggered cell to resolve Maxwell's equations so that the numerical results in the temporal dimension are almost identical to the precise solution. In contrast with the alternating-direction-implicit FDTD method, the first-order absorbing boundary condition can be introduced into this method successfully. Moreover, not only can it remove the Courant stability condition constraint, but also make the numerical dispersion independent of the time-step size.

In this paper, the extension of the precise integration time domain method to circular cylindrical coordinate system is presented. Such a

proposed method is particularly effective for solving axis-symmetric structures such as cylindrical antennas. The analytical proof of the unconditional stability is mentioned and numerical results are provided to validate the proposed method in the circular cylindrical coordinates.

The paper is organized in the following manner. In Section 2, the formulations of the precise integration time domain method for a two-dimensional (2-D) TM wave are presented. And related absorbing boundary condition is introduced into the method. In Section 3, a scheme is proposed for solving the noninvertible problem of the matrix $\boldsymbol{M}$ in the recursive scheme. In Section 4, the pertinent numerical results are shown. Finally, conclusions and discussions are made in Section 5.

## 2. PRECISE INTEGRATION TIME DOMAIN FORMULATIONS FOR A 2-D TM WAVE IN THE CIRCULAR CYLINDRICAL COORDINATE SYSTEM

In an isotropic lossless region with permittivity $\varepsilon$ and permeability $\mu$, the three scalar equations that relate the components of electric field $\boldsymbol{E}$ and magnetic field $\boldsymbol{H}$ in cylindrical coordinates can be readily obtained from Maxwell's equation. For instance,

$$\frac{1}{r}\frac{\partial(rH_\varphi)}{\partial r} = \varepsilon_0\frac{\partial E_z}{\partial t} \tag{2}$$

When treated with the finite-difference scheme, the above equation exists a singularity on the $r = 0$ because of the $1/r$ term. As a result, the cylindrical formulations have to be derived in two separate situations: one for the field components off the $r = 0$ axis and the other for the field components along the $r = 0$ axis.

### 2.1. The Formulations for Field Components off the $r = 0$ Axis

In this case, no singularity is presented. The principle as described in [18], can be directly applied to Equation (2), resulting in

$$\frac{dE_z(i, j+1/2)}{dt} = \frac{1}{\varepsilon_0 r_i}\frac{r_{i+1/2}H_\varphi(i+1/2, j+1/2) - r_{i-1/2}H_\varphi(i-1/2, j+1/2)}{\Delta r} \tag{3}$$

Equation (3) is the precise integration time domain formulation of the $E_z$ component off the $r = 0$ axis in computational domain in circular

cylindrical coordinates. The equations for the other components can be obtained in a similar way.

### 2.2. The Formulations for Field Components on the $r = 0$ Axis

In this case, as mentioned earlier, direct numerical updating of $E_z$ from Equation (2) is not feasible because of the $1/r$ term. To circumvent the difficulty, the following integral form of Maxwell's equation in the time domain is looked at and used

$$\oint_C H \cdot dl = \varepsilon \int_S \frac{\partial E}{\partial t} \cdot ds \tag{4}$$

Where $C$ is a closed contour surrounding the $r = 0$ axis, and $S$ is the surface bounded by the contour $C$.

By using the closed circular path of radius $\Delta r/2$ around the $r = 0$ axis, the following equation for $E_z$ at $r = 0$ can be obtained

$$\frac{dE_z(0, j + 1/2)}{dt} = \frac{4}{\varepsilon \Delta r} H_\varphi(1/2, j + 1/2) \tag{5}$$

Equation (5) is the precise integration time domain formulation of the $E_z$ components on the $r = 0$ axis in computational domain in circular cylindrical coordinates.

### 2.3. Absorbing Boundary Condition

Since the computational domain cannot include the whole space, the finite difference mesh must be truncated to accommodate the finite computer memories, i.e., the mesh must be limited in the $r$ and $z$ directions. The first-order absorbing boundary condition [19] is valid in the proposed method. The scalar equations that relate the components of electric field $\boldsymbol{E}$ or magnetic field $\boldsymbol{H}$ on the boundaries can be obtained from the cylindrical absorbing boundary condition. For instance,

$$\partial H_\varphi/\partial r + H_\varphi/(2r) + \partial H_\varphi/(c\partial t) = 0 \tag{6}$$

To obtain the discrete approximation to this partial differential equation, the central difference approximation is used on space first-order partial differentiation at an auxiliary grid-point $(I_{\max}, j + 1/2)$, i.e.,

$$\frac{dH_\varphi(I_{\max}, j+1/2)}{dr} = \frac{H_\varphi(I_{\max}+1/2, j+1/2) - H_\varphi(I_{\max}-1/2, j+1/2)}{\Delta r} \tag{7}$$

Assuming that

$$H_\varphi(I_{\max}, j{+}1/2) = (1/2)[H_\varphi(I_{\max}{+}1/2, j{+}1/2) + H_\varphi(I_{\max}{-}1/2, j{+}1/2)] \tag{8}$$

Substituting Equations (7) and (8) into Equation (6) gives

$$\frac{dH_\varphi(I_{\max}+1/2, j+1/2)}{dt} = 2c\left[-\frac{H_\varphi(I_{\max}{+}1/2, j{+}1/2) - H_\varphi(I_{\max}{-}1/2, j{+}1/2)}{\Delta r} - \frac{H_\varphi(I_{\max}, j{+}1/2)}{2r_{I\max}}\right] - \frac{dH_\varphi(I_{\max}{-}1/2, j{+}1/2)}{dt} \tag{9}$$

Substituting the precise integration time domain method form of the $H_\varphi$ component into Equation (9) gives

$$\begin{aligned}\frac{dH_\varphi(I_{\max}+1/2, j+1/2)}{dt} = & -2c\left[\frac{\begin{pmatrix}(r_{I\max}+(1/4)\Delta r)H_\varphi(I_{\max}+1/2, j+1/2)\\ -(r_{I\max}-(1/4)\Delta r)H_\varphi(I_{\max}-1/2, j+1/2)\end{pmatrix}}{\Delta r r_{I\max}}\right] \\ & + \frac{1}{\mu_0}\left[\frac{E_r(I_{\max}-1/2, j+1) - E_r(I_{\max}-1/2, j)}{\Delta z} - \frac{E_z(I_{\max}, j+1/2) - E_z(I_{\max}-1, j+1/2)}{\Delta r}\right]\end{aligned} \tag{10}$$

Equation (10) is the precise integration time domain form of the first-order absorbing boundary condition on the boundary $r = I_{\max}\Delta r$ for the field component $H_\varphi$. Similarly, such forms of the first-order boundary condition for all the other components can also be deduced in this way.

### 2.4. Precise Integration Technique for Solving the ODEs

With all of the ODEs both in the computational domain (like Equation (2)) and on the boundaries (like Equation (10)), we can summary them as a matrix form

$$\frac{d\boldsymbol{X}'}{dt} = \boldsymbol{M}'\boldsymbol{X}' \tag{11}$$

Where $\boldsymbol{X}'$ is a column vector containing the electric field and the magnetic field components defined on the discrete spatial grids, $\boldsymbol{M}'$

is a coefficient matrix. If some of the components are imposed to be at the certain values, the ODEs including the derivatives of these components with respect to $t$ should be deleted, and then we have

$$\frac{d\boldsymbol{X}}{dt} = \boldsymbol{M}\boldsymbol{X} + \boldsymbol{f}(t) \tag{12}$$

Where $\boldsymbol{f}(t)$ is a column vector introduced by excitation. When the inhomogeneous term $\boldsymbol{f}(t)$ is assumed to be linear within the time step $(t_n, t_{n+1})$, i.e.,

$$\boldsymbol{f}(t) = \boldsymbol{r}_0 + \boldsymbol{r}_1 \cdot (t - t_n) \tag{13}$$

The solution of Equation (12) is

$$\boldsymbol{X}_{n+1} = \boldsymbol{T}\left[\boldsymbol{X}_n + \boldsymbol{M}^{-1}\left(\boldsymbol{r}_0 + \boldsymbol{M}^{-1}\boldsymbol{r}_1\right)\right] - \boldsymbol{M}\left[\boldsymbol{r}_0 + \boldsymbol{M}^{-1}\boldsymbol{r}_1 + \boldsymbol{r}_1\tau\right] \tag{14}$$

Where $\boldsymbol{T} = \exp(\boldsymbol{M}\tau)$, and $\tau$ is the time step size. The matrix $\boldsymbol{T}$ can be computed by using the precise integration technique [18, 20]. With the technique, the solution of Equation (12) can be calculated with an accuracy of machine precision, i.e., no truncation error in the temporal dimension [18, 20].

### 2.5. Error and Stability Analyses

The error and the stability analyses of the precise integration time domain method in circular cylindrical coordinates are the same as those in Cartesian coordinates [18, 20].

## 3. SCHEME OF SOLVING NONINVERTIBLE MATRIX PROBLEM

Just like in Cartesian coordinates, the matrix $\boldsymbol{M}$ in cylindrical coordinates is also noninvertible in many cases. Hence, Equation (14) is unavailable directly. In order to solve this difficulty, elimination of unknowns is also discussed in this section.

### 3.1. In Computational Domain

Maxwell's equations show that all the components of electric field related to one node are linearly dependent, i.e., one of them can be expressed from the other components. The spatial discrete approximation is illustrated in Fig. 1, where the dielectric permittivity is $\varepsilon_0$.

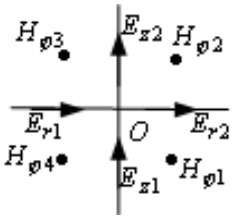


**Figure 1.** Spatial discretization of electric field components.

In the charge-free region, the precise integration time domain form of electric field components can be expressed as follows

$$\frac{dE_{z2}}{dt} = aH_{\varphi 2} - bH_{\varphi 3} \tag{15}$$

$$\frac{dE_{z1}}{dt} = aH_{\varphi 1} - bH_{\varphi 4} \tag{16}$$

$$\frac{1}{d}\frac{dE_{z2}}{dt} = -H_{\varphi 2} + H_{\varphi 1} \tag{17}$$

$$\frac{1}{d}\frac{dE_{r1}}{dt} = -H_{\varphi 3} + H_{\varphi 4} \tag{18}$$

Where $a = (r + \Delta r/2)/(\varepsilon_0 r\Delta r)$, $b = (r - \Delta r/2)/(\varepsilon_0 r\Delta r)$, $d = 1/(\varepsilon_0 \Delta z)$. Calculating the following equation $(15) + a \times (17) - (16) - b \times (18)$, and assuming that the initial condition is zero, we have

$$E_{z2} = E_{z1} - \frac{a}{d}E_{r2} + \frac{b}{d}E_{r1} \tag{19}$$

Equation (19) is the linear relation of electric components in computational domain in circular cylindrical coordinates.

### 3.2. On Absorbing Boundary

Fig. 2 shows the cells including the surface $r = r_{\max}$. On the surface $r = r_{\max}$, the precise integration time domain forms of the first-order boundary condition are given as

$$\frac{dH_{\varphi 1}}{dt} + \frac{dH_{\varphi 2}}{dt} = -2c\frac{a_1 H_{\varphi 1} - a_2 H_{\varphi 2}}{f} \tag{20}$$

$$\frac{dH_{\varphi 3}}{dt} + \frac{dH_{\varphi 4}}{dt} = -2c\frac{a_1 H_{\varphi 3} - a_2 H_{\varphi 4}}{f} \tag{21}$$

Where $a_1 = r_{\max} + \Delta r/4$, $a_2 = r_{\max} - \Delta r/4$, and $f = \Delta r r_{\max}$. And the precise integration time domain formulations of the $E_r$ and $E_z$

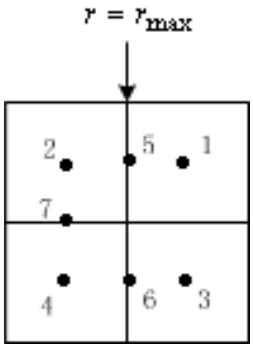


**Figure 2.** Spatial discretization near the surface $r = r_{\max}$.

components off the $r = 0$ axis are

$$\frac{dE_5}{dt} = \frac{1}{\varepsilon_0}\frac{b_1 H_{\varphi 1} - b_2 H_{\varphi 2}}{f} \tag{22}$$

$$\frac{dE_6}{dt} = \frac{1}{\varepsilon_0}\frac{b_1 H_{\varphi 3} - b_2 H_{\varphi 4}}{f} \tag{23}$$

$$\frac{dE_7}{dt} = -\frac{1}{\varepsilon_0}\frac{H_{\varphi 2} - H_{\varphi 4}}{\Delta z} \tag{24}$$

Where $b_1 = r_{\max} + \Delta r/2,\ b_2 = r_{\max} - \Delta r/2$. From Equations (20) and (22), we have

$$H_{\varphi 2} = -\frac{\varepsilon_0 f a_1}{a_1 b_2 - a_2 b_1}\frac{dE_5}{dt} - \frac{f b_1}{2c(a_1 b_2 - a_2 b_1)}\left(\frac{dH_{\varphi 1}}{dt} + \frac{dH_{\varphi 2}}{dt}\right) \tag{25}$$

Similarly, from Equations (21) and (23), Equation (26) can be obtained as follows

$$H_{\varphi 4} = -\frac{\varepsilon_0 f a_1}{a_1 b_2 - a_2 b_1}\frac{dE_6}{dt} - \frac{f b_1}{2c(a_1 b_2 - a_2 b_1)}\left(\frac{dH_{\varphi 3}}{dt} + \frac{dH_{\varphi 4}}{dt}\right) \tag{26}$$

Substituting Equations (25) and (26) into Equation (24) and assuming that the initial condition is zero gives

$$E_5 = E_6 - \frac{b_1}{2c\varepsilon_0 a_1}(H_{\varphi 1} + H_{\varphi 2} - H_{\varphi 3} - H_{\varphi 4}) + \frac{a_1 b_2 - a_2 b_1}{a_1 f}\Delta z E_7 \tag{27}$$

Equation (27) is the linear relation of electric field components on the absorbing boundary $r = r_{\max}$ in circular cylindrical coordinates.

## 4. NUMERICAL RESULTS

In order to test the developed cylindrical precise integration time domain algorithm, two numerical examples are computed. They are: 1) a thin-wire antenna and 2) a cylindrical cavity. The results are compared with those obtained using the FDTD and alternating-direction-implicit FDTD. For the sake of conciseness, we call the FDTD, alternating-direction-implicit FDTD, and precise integration time domain algorithms methods 1, 2, and 3, respectively, in this section.

### 4.1. Thin-wire Antenna

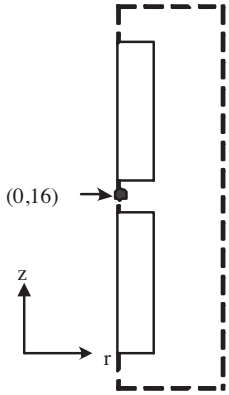


**Figure 3.** Model of a thin-wire antenna.

The model of a thin-wire antenna is shown in Fig. 3. The whole region is discretized with a uniform mesh. The size of the cells is set at 1 mm. The total number of the cells is $10\times31$. And the number of the cells in each of conductors is $2\times10$. The feeding gap of a wire antenna is modeled for calculation by the so-called "one-cell gap model" [6], which lets the feeding gap to be one spatial interval of Yee's lattice. $E_z(0,16)$ is excited with the rectangular pulse that is $E_{zs} = 1\,\mathrm{V/m}$ for $t \le t_0$ and $E_{zs} = 0$ for $t > t_0$, where $t_0 = 500\,\mathrm{ns}$. The conductivity of the thin-wire is $1\times10^7\,\mathrm{S/m}$. Inductivity of the model is set as $\varepsilon_r = 1.0$. The first-order absorbing boundary condition has been used.

The Courant stability condition is $\tau \le \Delta r/(2^{0.5}c) = 2.357\,\mathrm{ps}$ in this case, but the time-step size $\tau$ of the method 1 is set as $1\times10^{-11}\,\mathrm{s}$ in actual computation. The observation $E_r$-field is at the point $(7.5, 16)$, and the result of the method 1 is shown in Fig. 4. As can be seen, it quickly becomes unstable.

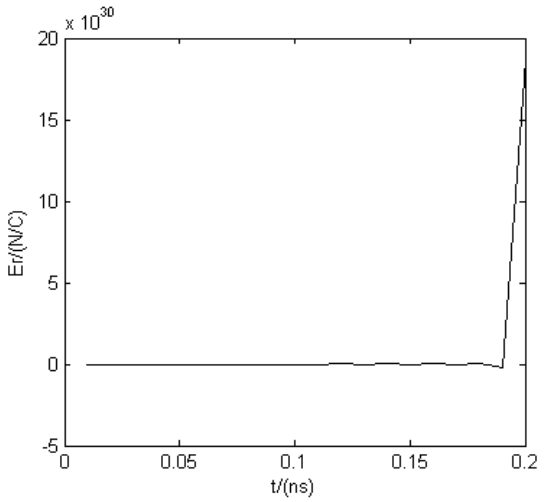


**Figure 4.** FDTD solution that becomes unstable.

Then $\tau$ is set as $1 \times 10^{-12}$ s for the method 1, and $1 \times 10^{-7}$ s for the method 3, respectively. The $E_r$-field components at the observation points $(7.5, 6)$, $(7.5, 16)$, and $(7.5, 28)$ are shown in Fig. 5. The method 3 remains quite stable even though the stability condition is not satisfied extremely. And the results of the method 3 and those of the method 1 are in quite good agreement.

Furthermore, it is necessary to compare the computation efficiency of the method 3 with the one of the method 1. Our simulations are performed on a CeleronM 1.7 GHz PC. The CPU times, the required memory sizes and the total time steps are shown in Table 1. In the case of the method 3, the time-step size can be set $10^5$ times as large as the method 1, the total time steps can be reduced by a factor of $10^5$, and the CPU time is also reduced to 1/2. Unfortunately, required memory size, which is about 37 times, is greatly increased because of the necessity for matrix storage.

**Table 1.** Information on the thin-wire antenna simulation.

| | Time-step size | Step number | CPU time | Memory requirement |
|---|---|---|---|---|
| Method 1 | $1 \times 10^{-12}$s | $5 \times 10^6$ | 220s | 0.8M |
| Method 3 | $1 \times 10^{-7}$s | 50 | 109s | 29.6M |

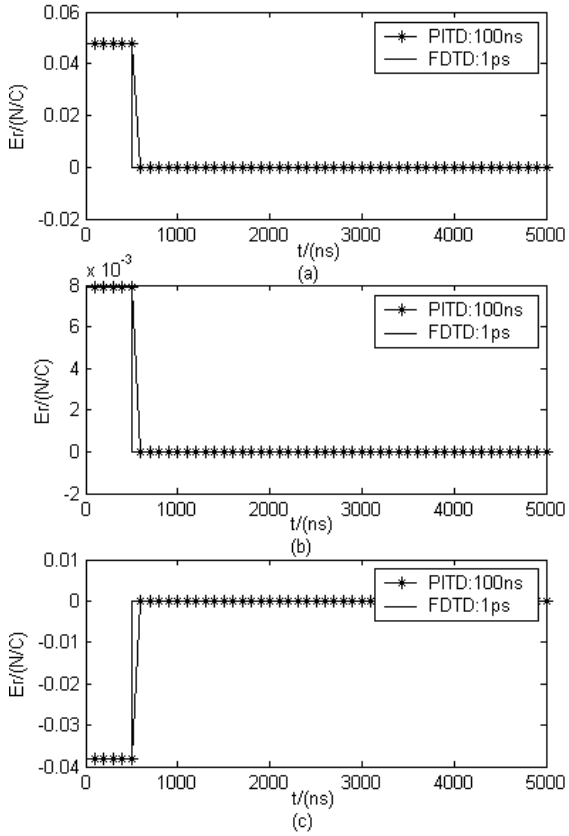


**Figure 5.** $E_r$-field in time domain (a) $E_r$-field at the observation point $(7.5, 6)$ (b) $E_r$-field at the observation point $(7.5, 16)$ (c) $E_r$-field at the observation point $(7.5, 28)$.

### 4.2. Cylindrical Resonant Cavity

As shown above, the method 3 is theoretically and numerically proved to be always stable, i.e., the selection of the time step size is then no longer restricted by stability. As a result, it is interesting and meaningful to investigate how the large time step size will affect computational accuracy.

Here an inhomogeneous cylindrical cavity is computed with the methods 1, 2, and 3, respectively. The cavity is $5\,\text{cm} \times 20\,\text{cm}$ in size, and filled with air. For the actual computation, a uniform mesh with $\Delta l = 1\,\text{cm}$ is used, leading to a mesh of $5 \times 20$ grid points. Besides the

method 1, the simulations are run for the cavity with the method 2 and the method 3 having a time step size that exceeds the limit defined by the Courant stability condition, $\tau_{\mathrm{FDTDTMAX}} = 2.357 \times 10^{-11}$ s here. $\tau = 1 \times 10^{-12}$ s is used with the method 1, $\tau = 1 \times 10^{-11}$ s with the method 2 and $\tau = 1 \times 10^{-11}$ s and $\tau = 6 \times 10^{-11}$ s with the method 3. $E_r(0.5, 10)$ is excited with the rectangular pulse that is $E_{rs} = 1\,\mathrm{V/m}$ for $t \leq t_0$ and $E_{rs} = 0$ for $t > t_0$, where $t_0 = 1.2 \times 10^{-9}$ s. Fig. 6 shows the $E_r$-field at the observation points $(0.5, 16)$, $(0.5, 4)$ and $(2.5, 10)$. As can be seen, the method 3 remains with the stable solution. And all the results of the method 3 are much closer to the ones of the method 1, but those of the method 2 are not.

Now we investigate how the large time step size will have an effect on the computation accuracy. For comparative purposes, both the methods 2, and 3 are used to simulate the cavity. Table 2 presents the simulation results for the $\mathrm{TM}_{113}$ mode in the cavity. The analytical

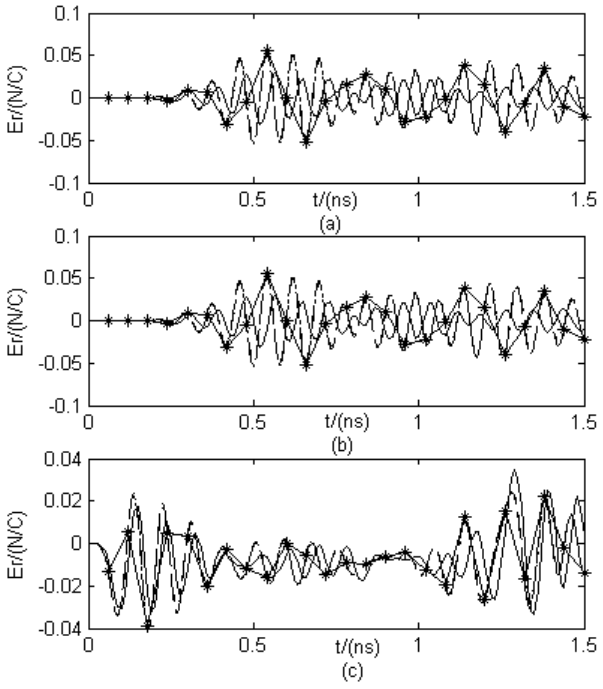


**Figure 6.** Time-domain $E$-field at different observation points (Dashdot line - method 3 $\tau = 10\,\mathrm{ps}$, Solid line with stars - method 3 $\tau = 60\,\mathrm{ps}$, Dashed line - method 1 $\tau = 1\,\mathrm{ps}$, Solid line - method 2 $\tau = 10\,\mathrm{ps}$) (a) $(0.5, 16)$, (b) $(0.5, 4)$, (c) $(2.5, 10)$.

result of the $TM_{113}$ mode is 4.296 GHz [21]. As can be seen, the relative errors of the method 3 will not increase with the time step.

**Table 2.** The simulation results of methods 2 and 3 with different time-step size $\tau_i$ for the $TM_{113}$ mode.

| | $\tau_1$= 40ps | | $\tau_2$= 60ps | | $\tau_3$= 80ps | |
|---|---|---|---|---|---|---|
| | Result (GHz) | Relative error | Result (GHz) | Relative error | Result (GHz) | Relative error |
| Method 3 | 4.302 | 0.140% | 4.302 | 0.140% | 4.302 | 0.140% |
| Method 2 | 4.042 | 5.912% | 3.776 | 12.10% | 3.490 | 18.76% |

Fig. 7 illustrates the relative errors for the $TM_{113}$ mode of the cavity computed using the method 2 and the method 3 with variable time steps. For clearness, the relative time-step $\tau/\tau_{\mathrm{FDTDTMAX}}$ is used. As can be seen, at the lower $\tau/\tau_{\mathrm{FDTDTMAX}}$, the errors of both the method 2 and the method 3 are almost the same. However, for $\tau/\tau_{\mathrm{FDTDTMAX}} > 1.0$, the error of the method 2 increases with the growth of the time-step size $\tau$, while the method 3 continues to produce stable results with the same errors.

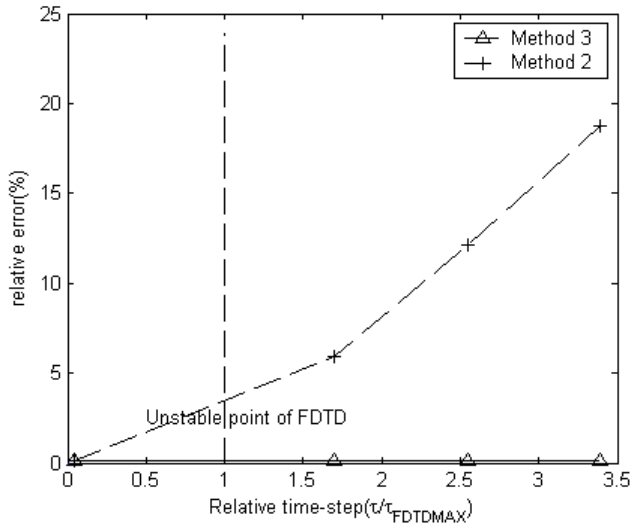


**Figure 7.** Relative errors of the method 2 and the method 3 as the function of relative time step size.

Table 3 shows the five resonant frequencies obtained with methods 1, 2, and 3, respectively. $\tau = 1\,\text{ps}$ is used with the method 1, and 40 ps with the methods 2 and 3. The errors of the methods 1 and 3 are identical, but smaller than the ones of the method 2.

**Table 3.** Resonant frequencies obtained with the methods 1, 2, and 3.

| Analytic | Method 1 | | Method 2 | | Method 3 | |
|---|---|---|---|---|---|---|
| Results (GHz) | Results (GHz) | Relative Error | Results (GHz) | Relative Error | Results (GHz) | Relative Error |
| 2.416 | 2.391 | 1.035% | 2.331 | 3.518% | 2.391 | 1.035% |
| 3.215 | 3.182 | 1.026% | 3.078 | 4.261% | 3.182 | 1.026% |
| 4.296 | 4.302 | 0.140% | 4.042 | 5.912% | 4.302 | 0.140% |
| 5.324 | 5.479 | 2.911% | 4.922 | 7.550% | 5.479 | 2.911% |
| 6.065 | 6.198 | 2.192% | 5.646 | 6.908% | 6.198 | 2.192% |

For comparative purposes of the computation efficiency, the methods 1, 2, and 3 are used to simulate the cavity again. Here, the time-step size $\tau = 1 \times 10^{-12}\,\text{s}$ is used with the method 1, the $\tau = 2 \times 10^{-12}\,\text{s}$ is used with the method 2, while $\tau = 4 \times 10^{-11}\,\text{s}$ is used with the method 3. With such selection of the time step sizes, we find that the three methods present almost same accuracy. Therefore, the three methods can be compared in a fair manner. Table 4 shows the five resonant frequencies obtained with the three methods. The errors for the three methods are almost the same.

The simulation is performed on a CeleronM 1.7 GHz PC. Table 5 provides some information on this simulation. For the method 3, when the time-step size is set at 20 times as large as that of the method 2, the total time steps can be reduced by a factor of 20, and the CPU time is reduced to 46.2%. The time-step size of the method 3 can be set at 40 times as large as the method 1, the total time steps can be reduced by a factor of 40, and the CPU time is also reduced to 17.1%.

**Table 4.** Resonant frequencies obtained with the methods 1, 2, and 3.

| Analytic | Method 1 | | Method 2 | | Method 3 | |
|---|---|---|---|---|---|---|
| Results (GHz) | Results (GHz) | Relative Error | Results (GHz) | Relative Error | Results (GHz) | Relative Error |
| 2.416 | 2.391 | 1.035% | 2.391 | 1.035% | 2.391 | 1.035% |
| 3.215 | 3.182 | 1.026% | 3.182 | 1.026% | 3.182 | 1.026% |
| 4.296 | 4.302 | 0.140% | 4.302 | 0.140% | 4.302 | 0.140% |
| 5.324 | 5.479 | 2.911% | 5.479 | 2.911% | 5.479 | 2.911% |
| 6.065 | 6.198 | 2.192% | 6.198 | 2.192% | 6.193 | 2.110% |

**Table 5.** Information on the cylindrical resonant cavity simulation.

| | CPU time | Memory requirement | Time-step size | Step number |
|---|---|---|---|---|
| Method 1 | 35s | 1M | $1 \times 10^{-12}$s | $1.92 \times 10^5$ |
| Method 2 | 13s | 1.8M | $2 \times 10^{-12}$s | $9.6 \times 10^4$ |
| Method 3 | 6s | 4M | $4 \times 10^{-11}$s | 4800 |

## 5. CONCLUSION

A precise integration time domain method in circular cylindrical coordinate system free of the Courant stability condition has been presented in this paper. The Yee's grid is used and the precise integration technique is applied to formulate the algorithm. In comparison with its counterpart of Cartesian coordinate system, the proposed method needs to carry out an additional special treatment of the singularity of the $1/r$ term on the axis $r = 0$. Moreover, the linear relations leading to the matrix $\boldsymbol{M}$ being noninvertible are found and the unknown-elimination is applied to realize the recursive scheme. Analytical proof of the unconditional stability is mentioned and the numerical simulation results are presented to validate the proposed method and to demonstrate its effectiveness. In the first example, it is found that the precise integration time domain method

can achieve up to 50% times of saving in CPU time in comparison with the FDTD method. And the second experiment indicates that with the same accuracy, it uses 20 times less iteration and is 2.2 times faster than the alternating-direction- implicit FDTD. However, the memory requirement of the proposed method is much larger than those of the FDTD and the alternating-direction-implicit FDTD methods, that is to say, further investigations on different computer-memory-saving schemes will make the precise integration time domain method more suitable for computer-aided design (CAD) purposes.

## REFERENCES

1. Yee, K. S., "Numerical solution of initial boundary value problems involving Maxwell's equations in isotropic media," *IEEE Trans. Antennas Propagat.*, Vol. 14, 302–307, 1966.
2. Gong, Z. and G.-Q. Zhu, "FDTD analysis of an anisotropically coated missile," *Progress In Electromagnetics Research*, PIER 64, 69–80, 2006.
3. Gao, S., L.-W. Li, and A. Sambell, "FDTD analysis of a dual-frequency microstrip patch antenna," *Progress In Electromagnetics Research*, PIER 54, 155–178, 2005.
4. Young, J. L. and R. Adams, "Excitation and detection of waves in the fdtd analysis of n-port networks," *Progress In Electromagnetics Research*, PIER 53, 249–269, 2005.
5. Chen, X., K. Huang, and X.-B. Xu, "Microwave imaging of buried inhomogeneous objects using parallel genetic algorithm combined with fdtd method," *Progress In Electromagnetics Research*, PIER 53, 283–298, 2005.
6. Taflove, A., *Computational Electromagnetics: The Finite-Difference Time-Domain Method*, 637, Artech House, MA, 1996.
7. Dib, N., T. Weller, and M. Scardelletti, "Analysis of 3-D cylindrical structures using the finite-difference time-domain method," *IEEE MTT-S Int. Microwave symp. Dig.*, 925–928, Baltimore, MD, 1998.
8. Chen, Y., R. Mittra, and P. Harms, "Finite-difference time-domain algorithem for solving Maxwell's equations in rotationally symmetric geometries," *IEEE Trans. Microwave Theory and Techniques*, Vol. 44, 832–839, 1996.
9. Zheng, F. H., Z. Z. Chen, and J. Z. Zhang, "A finite-difference time-domain method without the Courant stability conditions," *IEEE Microwave and Guided Wave Letters*, Vol. 9, 441–443, 1999.
10. Namiki, T., "A new FDTD algorithm based on alternating-

direction implicit method," *IEEE Trans. Microwave Theory and Techniques*, Vol. 47, 2003–2007, 1999.

11. Zhen, F. H. and Z. Z. Chen, "Numerical dispersion analysis of the unconditionally stable 3-D ADI-FDTD method," *IEEE Trans. Microwave Theory and Techniques*, Vol. 49, 1006–1009, 2001.
12. Kermani, M. H., X. Wu, and O. M. Ramahi, "Instable ADI-FDTD open-region simulation," *IEEE A P-S Int. Symp.*, Vol. 1, 595–598, 2004.
13. Kermani, M. H. and O. M. Ramahir, "Instable 3D ADI-FDTD open-region simulation," *IEEE A P-S Int. Symp.*, Vol. 1B, 142–145, 2005.
14. Zhao, J. Q., X. K. Ma, Y. P. Li, and G. Y. Qiu, "Analysis of the electromagnetic transient of multiphase transmission lines by the precise integration method," *Journal of High-Voltage Technology*, Vol. 27, 3–4, 2001 (in Chinese).
15. Tang, M. and X. K. Ma, "A precise integration algorithm for transient simulation of interconnects in high-speed VLSI," *Journal of Electronics*, Vol. 32, 787–790, May 2004 (in Chinese).
16. Yang, M. and X. K. Ma, "A semi-integral method for the calculation of electromagnetic pulse propagation in ferromagnetic sheet," *Transactions of China Electrotechnical Society*, Vol. 20, 89–94, 2006 (in Chinese).
17. Zhao, X. T. and X. K. Ma, "An unconditionally stable time domain method based on precise integration," *Record of the 15th COMPUMAG CONFERENCE on the Computation of Electromagnetic Field*, 204–205, Shenyang, China, June 26–30, 2005.
18. Ma, X. K., X. T. Zhao, and Y. Z. Zhao, "A 3-D precise integration time-domain method without the restraints of the Courant-Friedrich-Levy stability condition for the numerical solution of Maxwell's equations," *IEEE Trans. Microwave Theory and Techniques*, Vol. 54, 3026–3037, 2006.
19. Ge, D. B. and Y. B. Yan, *The Finite Difference Time Domain Method for Electromagnetic Wave*, 169–173, Xidian University Press, Xi'an, 2002.
20. Zhong, W. X. and F. W. Williams, "A precise time-step integration method," *Proceedings of the Institution of Mechanical Engineers Part C-Journal of Mechanical Engineering Science*, Vol. 208, 427–430, 1994.
21. Pozar, D. M., *Microwave Engineering*, 350, Addison-Wesley, MA, 1990.